Nanoscale

Twisted 1T TaS2 Bilayers by Lithiation Exfoliation

Journal:	*Nanoscale*
Manuscript ID	NR-COM-07-2020-005148.R1
Article Type:	Communication
Date Submitted by the Author:	07-Aug-2020
Complete List of Authors:	Li, Hui; Shanghai Jiao Tong University Liu, Pan; WPI-AIMR, ; Shanghai Jiao Tong University, Liu, Qi; Beijing Computational Science Research Center, Luo, Ruichun; Shanghai Jiao Tong University Guo, Chenguang; CAS Key Laboratory of Materials for Energy Conversion, Shanghai Institute of Ceramics, Chinese Academy of Sciences, Wang, Ziqian; Johns Hopkins University Guan, Pengfei; CSRC Florencio Aleman, Christopher ; Johns Hopkins University, Huang, Fu Qiang; Shanghai Institute of Ceramics Chinese Academy of Sciences, Chen, Mingwei; Johns Hopkins University, Materials Science and Engineering; Tohoku University, WPI-AIMR

SCHOLARONE™
Manuscripts

Twisted 1T TaS_2 Bilayers by Lithiation Exfoliation

Hui Li[1], Pan Liu[1*], Qi Liu[2], Ruichun Luo[1], Chenguang Guo[3], Ziqian Wang[4], Pengfei Guan[2], Christopher Florencio Aleman[4], Fuqiang Huang[3], Mingwei Chen[4]*

[1]State Key Laboratory of Metal Matrix Composites, School of Materials Science and Engineering, Shanghai Jiao Tong University, Shanghai, 200030, China

[2]Beijing Computational Science Research Center, Beijing 100084, China

[3]State Key Laboratory of High Performance Ceramics and Superfine Microstructure, Shanghai Institute of Ceramics, Chinese Academy of Sciences, Shanghai 200050, China

[4]Department of Materials Science and Engineering, Johns Hopkins University, Baltimore , MD 21214 , USA

*E-mail: panliu@sjtu.edu.cn, mwchen@jhu.edu

Abstract:

We report twisted 1T TaS_2 bilayers synthesized by a lithiation exfoliation method. Atomic-scale observations reveal the existence of eight twist commensurate configurations from over 50 1T TaS_2 bilayer samples in the twist angle range from 0° to 30° in which commensurate atomic configurations can be distinguished by scanning transmission electron microscopy. The limited number of twist angles, rather than random ones, indicates that there are energetically favorite twist angles in the naturally formed bilayers. Together with the interlayer distance measurements, the formation of the bilayer twist configurations is anticipated to be regulated by the

stacking energy in the charge-density-wave system through interlayer van der Waals interactions. The findings of this work may pave a new way to fabricate twisted bilayer TMDs for exploring exotic properties from additional moiré periodicity.

Key Words: 2D materials, twisted TaS_2 bi-layers, scanning transmission electron microscopy, moiré pattern, commensuration

Introduction

Two dimensional (2D) van der Waals (vdW) materials, such as transition metal dichalcogenides (TMDs), provide a unique opportunity to assemble new materials by sequentially stacking monolayers[1]. The design of the stacking sequence, the selection of constituent materials, and the twist of azimuthal orientations between layers have been successfully utilized to explore new functionalities of 2D materials, such as superconductivity[2], irreplaceable optoelectronic behavior[3], and emergent electronic states[4-6]. 1T TaS_2 is a typical vdW TMD material and can be fabricated in the form of one-unit-cell-thick 2D crystals by mechanical exfoliation[7, 8], chemical exfoliation[9-11], or chemical vapor deposition[12]. It has been known for a long time that bulk 1T TaS_2 is a prototypical charge-density-wave (CDW) material that spontaneously breaks lattice symmetry through periodic lattice distortions (PLDs)[13]. The metallic 1T TaS_2 undergoes a series of CDW transitions at temperatures below 543 K until it finally enters a Mott insulator state below 180 K where the CDW concomitant PLDs becomes commensurate with the crystal lattices[14, 15]. Therefore, the commensuration of mismatch lattices could be an important factor for tailoring physical properties of 1T TaS_2. It has been suggested that 1T TaS_2 monolayers have the same PLD as the bulk counterpart. Similarly, they are Mott insulators with a S=1/2 degree of freedom in each unit cell while the bilayers with zero twist angle form a singlet state and are antiferromagnetic insulators with opposite spins by the interlayer interactions.[16, 17] Naturally, it can be anticipated that additional periodicities generated from twist stacking of commensurate 1T TaS_2 monolayers may alter the metal to Mott insulator

transition and offer new physical properties. Recently, density of state (DFT) calculations predicted that the electronic properties of TaS_2 bilayers strongly depend on the twist angles[18]. The twisted 1T TaS_2 bilayers experience a transition from metal to semiconductor between 27.8° and 32.2° and their CDW gaps increase with the twisted angles. However, twisted TaS_2 bilayers with various azimuthal angles have not been experimentally realized. In this study, we report the fabrication of twisted 1T TaS_2 bilayers by a lithiation exfoliation method. Cs-corrected scanning transmission electron microscopy (STEM) reveals the energetically favorite twist angles in 1T TaS_2 bilayers and the correlation between twist angles and interlayer distances.

Sample preparation and characterization of twisted bilayer TaS_2.

The 1T-TaS_2 crystalline powders were synthesized by stoichiometric elements of Ta (99.9% purity) and S (99.999%) in an evacuated quartz tube at 800 to 900°C for 10 days. The obtained 0.1 g 1T-TaS_2 precursors were soaked in 20 mL of 1.6 M n-butyllithium in hexane for 3 days and then washed with pure hexane three times before drying under an evacuated condition. The resulting $LiTaS_2$ powders were soaked in distilled water and sonicated for 30 min with stirring until the mixture became a transparent dispersion solution of exfoliated TaS_2 nanosheets. Finally, the obtained uniform dispersion solution was dialyzed repeatedly to completely remove Li ions from the solution and 1T TaS_2 nanosheets were obtained through air pump filtration. The TaS_2 nanosheets have irregular shapes and the lateral dimensions are about several to tens of micrometers in the longest direction. The thicknesses of

nanosheets were characterized by atomic force microscopy (see **Figure S1**). The binding states and quantitative chemical compositions of the pristine TaS2 nanosheets were investigated by X-ray photoelectron spectroscopy (XPS) (**Figure S2**). The Ta $4f_{7/2}$ and S $2p_{3/2}$ spectra demonstrate that the liquid-exfoliated nanosheets keep the stoichiometry of the precursor TaS_2 compound. The weak XPS peaks from Ta_2O_5 demonstrate that the oxidation of the as prepared TaS_2 nanosheets is insignificant. With this processing, most of the samples are bilayers, together with a small number of mono and tri-layers. In contrast, a relatively dilute 1T-TaS_2 solution leads to the formation of monolayer-dominated nanosheets. The structure of the as-prepared individual TaS_2 nanosheets was characterized by high-angle annular dark field (HAADF) STEM using Cs-corrected TEMs (JEOL 2100F and ARM 200F) with a spherical aberration (Cs) corrector for the condense lens at the accelerating voltage of 200 kV. HAADF-STEM images were acquired with inner and outer collection angles of 50-150 mrad, respectively. All images were acquired with a 20 μs dwell time at the convergence semi-angle of 16 mrad, giving a probe size of ~1 Å and a beam current of 30 pA.

Structure of 1T-TaS_2 bilayer with different twist angles

The structure of the as-prepared TaS_2 nanosheets was characterized by HAADF-STEM. In the atomic image and corresponding intensity profile (**Figure 1a**), the atomic columns with a bright contrast are from Ta while the contrast of solo S atoms has a very low intensity, as shown in the intensity profile. The schematic

atomic model for the 1T structure is displayed in **Figure 1b** with the yellow color representing the top layer S atoms, blue for the middle layer Ta atoms, and purple for the bottom layer S atoms. The Ta atoms form a triangular lattice sandwiched between two triangular layers of S with the stacking sequence of A-B-C in one-unit thickness. Hence, Ta atoms have an octahedral coordination with S atoms in the 1T phase which is fundamentally different from the 2H structure in which Ta atoms have a trigonal prismatic coordination with S atoms[19, 20]. The 1T structure of the as-prepared TaS_2 nanosheets is further confirmed by X-ray diffraction (**Figure 1c**). The X-ray peaks acquired from as-prepared TaS_2 nanosheets well match the reference lines at bottom representing 1T-TaS_2 data taken from the PDF database No. 02-0137.

We noticed that Moiré patterns can be frequently observed from these as-prepared 2D nanosheets, implying that twist-stacking takes places during the sample preparation process. **Schematic 1** illustrates the atomic model of two monolayer TaS_2 sheets, which are vertically stacked with a twist angle α to form a twist-stacking structure with a two-dimensional Moiré pattern. In principle, the α values could be any arbitrary azimuthal angle for the sequentially stacking non-lattice matched monolayers. However, only eight configurations can be frequently observed when we inspected about fifty bilayer TaS_2 nanosheets. These configurations with different twist angles are summarized in **Figure 2a-h**, including the known 1T phase in bulk TaS_2 and seven Moiré phases with the twist angles of 5.4°, 6.5°, 7.4°, 16.4°, 18.9°, 25.0° and 30.5°. The measured angle error is smaller than 0.1° (see **Figure S3**). The twist bilayer sample generally lay flat over large regions with a consistent twist angles as

verified by selected area electron diffraction (**Figure S4a)**. For the standard ABC stacking of S-Ta-S in the unit cell (**Figure 2a),** the trigonal arrangement of Ta atoms is observed from the HAADF-STEM image, which can be expected from the stacking of the Ta atoms from each layer directly atop each other. The twist angles were measured from fast Fourier transform (FFT) patterns of the atomic-scale HAADF-STEM images. Each [0001] FFT patterns contains twelve {1-100) spots, which constitute two hexagons as illustrated in the insets of **Figure 2b-h**. It worth noting that the configurations with the twist angles between 30° to 60° cannot be distinguished because the rotation angles of α and (60°-α) produce the identical HAADF-STEM images of Ta atoms and corresponding FFT patterns.

Figure S5 shows the frequency of each twist angle observed out of 50 examined bilayer 1T-TaS_2 nanosheets. 32 out of 50 nanosheets have the twist angle of 0° or 60°, which also have the smallest interlayer distance of 0.616 nm. For the interlayer distance measurement, it will be detailed later. Among the 18 twisted bilayer samples, 16.4° has highest frequency and the largest interlayer distance of 0.664 nm, while 25° and 30.5° are only observed one time each and have a related smaller interlayer distance of ~0.65 nm. We have to admit that the observations may miss some configurations with the twist angles out of the eight cases and the sampling size may not large enough for reliable statistical analysis. However, even from the current data, we can find that the probabilities of the twist angles are not equal and random and there are geometrically favorite twist angles in the naturally formed bilayers. The preferred twist angles might be energetically selected by the interlayer vdW interactions.

To understand the structure of the twist-stacked TaS_2 bilayers, the corresponding atomic models are constructed with the twist angles determined by the FFT measurements (**Figure 3**). Compared to the measured twist angles in experiments, the differences may be from measuring errors. These geometric models show the super-periodic Moiré patterns from the real-space projections. We used these atomic models to simulate HAADF-STEM images by the HREM software package, which is based on the multislice method[21]. This method has been widely employed to simulate HAADF-STEM images, including 1T TMD nanosheets[22]. For the 1T-TaS_2 monolayers, the simulated image (**Figure 4a)** has an excellent match with the corresponding HAADF-STEM image in both symmetry and lattice constant. We noticed that there are local lattice deviations in some regions between the simulated and experimental images, which could be associated with the PLD of the 1T phase or possible local reconstruction driven by the stacking energy. The lattice spacing of 2.86 Å is assigned to the (10-10) plane of 1T-TaS_2. The average lattice spacings measured from the HAADF-STEM images are very close to this value with a small error bar of +/- 5 pm. **Figure 4b** depicts the simulated HAADF-STEM images from the atomic model of the twisted TaS_2 bilayer with a small angle of 5.2°. Consistent with the HAADF-STEM image, the superposition of two identical layers with the small twist angle gives rise to an additional large periodicity. The simulated image is well consistent with the experimental one (**Fig. 4b**) in both Ta atomic positions and the Moiré pattern, verifying the correlation between the twist angle and the Moiré patterns suggested by FFT analysis and the structural models. We also used the same

methodology to simulate the twist-stacking configurations with the angles of 6.6°, 7.5°, 16.1°, 19.1°, 25.3 and 30°, respectively. With the increase of the twist angles, the size of the Moiré patterns gradually decreases, in line with the experimental observations. The models and the simulated images (**Figure 4c-h)** also confirm the twist angles of the Moiré patterns, which are measured from the FFT patterns, and the structural origins of the Moiré patterns observed in the HAADF-STEM images from the superposition between two vertically stacked TaS_2 monolayers with the misalignment by rotation.

In addition, the bilayer structures can be verified from the HAADF-STEM images taken from the folded edges of the samples as shown in **Figure 5**. Two parallel lines in the HAADF-STEM images represent two stacking TaS_2 monolayers. To better exhibit the geometry of curled twist bilayer TaS_2, we prepared a schematic diagram to show the folded structure near the edge (**Figure S6**). We measured the interlayer distances of these samples from the intensity profiles that were extracted along the direction perpendicular to the edges. The measured spacing error is ~0.17 Å (see **Figure S6**). As shown in **Figure 5i,** the general tendency that the interlayer distance increases with the twist angles is in line with the DFT calculations[18], indicating that the vdW interactions between the two twist layers change with the twist angles. Importantly, our experimental measurements suggest that the increment of the interlayer distance is not monolithic. There are two obvious plateaus at 6.5° and 25.0°. Since the interlayer distances directly correlate with the interlayer interactions and stacking energy, the uneven interlayer distances may be related to the structural relaxation and reconstruction

in the twisted bilayers [6, 23]. Therefore, the twist stacking of the 1T TaS_2 is anticipated to be an effective approach to modify the electronic structure and properties of 2D TaS_2 as well as to fabricate metastable CDW phases with unique properties.

Relationship between twist angle and commensurate structure

To further understand the geometric relations between twist angles and the resulting Moiré patterns observed by HAADF-STEM, we can derive the conditions required on the twist angles such that the system is commensurate for the formation of the Moiré patterns. Let $\overrightarrow{a_1}$ and $\overrightarrow{a_2}$ be the Bravais lattice vectors of a single TaS_2 layer as illustrated in **Figure 1b**. Then, the position vector of any Ta lattice point on this TaS_2 layer can be written as $m_1\overrightarrow{a_1}+m_2\overrightarrow{a_2}$ where m_1 and m_2 are integers. Now suppose we stack another TaS_2 layer on top with a twist angle α. We now seek the exact same feature somewhere else in the twisted bilayer TaS_2 whose position vector we can write as $n_1\overrightarrow{a_1}+n_2\overrightarrow{a_2}$ where n_1 and n_2 are integers. If the structure is commensurate, the two vectors must be related via a rotation i.e.

$$m_1\overrightarrow{a_1} + m_2\overrightarrow{a_2} = R(n_1\overrightarrow{a_1} + n\overrightarrow{a_2}) \quad (1)$$

where R is a rotation matrix, and can be written in Cartesian coordinates as[24]:

$$R = \begin{bmatrix} \cos\partial & -\sin\partial \\ \sin\partial & \cos\partial \end{bmatrix} \quad (2)$$

However, it would be more illuminating to re-write the rotation matrix R using the TaS_2 Bravais lattice vectors $\overrightarrow{a_1}$, $\overrightarrow{a_2}$ as our basis. In this basis,

$$R = \begin{bmatrix} \cos(\partial) - \frac{1}{\sqrt{3}}\sin(\partial) & -\frac{2}{\sqrt{3}}\sin\partial \\ \frac{2}{\sqrt{3}}\sin\partial & \cos(\partial) + \frac{1}{\sqrt{3}}\sin(\partial) \end{bmatrix} \quad (3)$$

Since m_1, m_2, n_1, n_2 are all integers, enforcing the commensurability conditions require all the entries of R in the Bravais lattice to be rational. This leads to a set of twist angles for which the twisted bilayer TaS_2 is a commensurable structure:

$$\cos(\alpha) = \frac{3q^2 - p^2}{3q^2 + p^2} \quad p,q \in Z \tag{4}$$

A series of twist angles α that satisfy equation (4) are calculated and listed in **Table 1**, with q equal to integers from 1 to 20 and p equal to integers from 1 to 10. The twist angles above 60° are ignored. All experimentally observed twisted angles can be found in **Table 1** as highlighted in grey, within 0.2° difference which are considered as the experimental error. This illustrates that the configurations of all the experimentally observed twisted TaS_2 bilayers are commensurate. However, as indicated in **Table 1**, there are a large number of other commensurate configurations in the TaS_2 system which have not been found in our extensive TEM observations. This implies that the twist angles of the as-prepared bilayers could be energetically favorite and regulated by the stacking energy during the formation of the twisted bilayers.

The resulting commensurate basic vectors of twist bilayers can be written in two classes according to δ=3/gcd(p,3) (here gcd is the greatest common divisor)[25]

For δ=1,

$$\vec{t_1} = \frac{1}{\gamma}\left[-(p+3q)\vec{a}_1 - 2p\vec{a}_2\right] \tag{5}$$

$$\vec{t_2} = \frac{1}{\gamma}\left[2p\vec{a}_1 - (p-3q)\vec{a}_2\right] \tag{6}$$

For δ=3,

$$\vec{t_1} = \frac{1}{\gamma}\left[-(p+q)\vec{a}_1 + 2q\vec{a}_2\right] \tag{7}$$

$$\vec{t_2} = \frac{1}{\gamma}\left[-2q\vec{a}_1 - (p-q)\vec{a}_2\right] \tag{8}$$

where γ=gcd(p+3q, p-3q). The calculated basic vectors of moiré unit cell with observed twist angles are listed in **Table 2**. The basic vectors of moiré unit cell with 16.4° were label on the HAADF-STEM image as shown in **Figure 6**. Since the digital scanning time of 19.1 μs per pixels was used, the total intake time is about 4 seconds for taking the HAADF-STEM image. It is unavoidable that the sample drift along the x- and y-coordinate directions during image acquirement. Even so, the calculated vectors matches well with the Ta atom periodicity in the HAADF-STEM images, confirming that the configurations of all the experimentally observed twisted TaS_2 bilayers are commensurate and the arrangement of the atoms within each moiré period are periodic.

Summary

In summary, we report that the twisted 1T TaS_2 bilayers can be synthesized by the lithiation exfoliation method. From HAADF-STEM observations, we found that the twist angles in the naturally formed 1T TaS_2 bilayers have defined values, not stochastic. Only eight configurations with the twist angles of 0°, 5.4°, 6.5°, 7.4°, 16.4°, 18.9°, 25.0°, 30.5° are observed from fifty samples with STEM distinguishable twist configurations. This may indicate that the formation of twisted bilayered structures may be energetically governed by the interlayer interactions and stacking energy. The simulated HAADF-STEM images from the atomic models well represent the Moiré patterns shown in the experimental ones. Geometric analysis demonstrates that these configurations are commensurate.

References

1. A. K. Geim and I. V. Grigorieva, *Nature*, 2013, **499**, 419-425.
2. Y. Cao, V. Fatemi, S. Fang, K. Watanabe, T. Taniguchi, E. Kaxiras and P. Jarillo-Herrero, *Nature*, 2018, **556**, 43-50.
3. K. Tran, G. Moody, F. Wu, X. Lu, J. Choi, K. Kim, A. Rai, D. A. Sanchez, J. Quan, A. Singh, J. Embley, A. Zepeda, M. Campbell, T. Autry, T. Taniguchi, K. Watanabe, N. Lu, S. K. Banerjee, K. L. Silverman, S. Kim, E. Tutuc, L. Yang, A. H. MacDonald and X. Li, *Nature*, 2019, **567**, 71-75.
4. H. Yu, G.-B. Liu, J. Tang, X. Xu and W. Yao, *Science Advances*, 2017, **3**, e1701696.
5. A. M. van der Zande, J. Kunstmann, A. Chernikov, D. A. Chenet, Y. You, X. Zhang, P. Y. Huang, T. C. Berkelbach, L. Wang, F. Zhang, M. S. Hybertsen, D. A. Muller, D. R. Reichman, T. F. Heinz and J. C. Hone, *Nano Letters*, 2014, **14**, 3869-3875.
6. M. R. Rosenberger, H.-J. Chuang, M. Phillips, V. P. Oleshko, K. M. McCreary, S. V. Sivaram, C. S. Hellberg and B. T. Jonker, *ACS Nano*, 2020, 14, 4550-4558.
7. H. Li, G. Lu, Y. Wang, Z. Yin, C. Cong, Q. He, L. Wang, F. Ding, T. Yu and H. Zhang, *Small*, 2013, **9**, 1974-1981.
8. K. S. Novoselov, D. Jiang, F. Schedin, T. J. Booth, V. V. Khotkevich, S. V. Morozov and A. K. Geim, *Proceedings of the National Academy of Sciences of the United States of America*, 2005, **102**, 10451-10453.
9. X. Li, C. y. Kim, S. Lee, D. Lee, H.-M. Chung, G. Kim, S.-H. Heo, C. Kim, K.-S. Hong and J. Yoon, *Journal of the American Chemical Society*, 2017, **139**, 10880-10886.
10. J. N. Coleman, M. Lotya, A. O'Neill, S. D. Bergin, P. J. King, U. Khan, K. Young, A. Gaucher, S. De, R. J. Smith, I. V. Shvets, S. K. Arora, G. Stanton, H.-Y. Kim, K. Lee, G. T. Kim, G. S. Duesberg, T. Hallam, J. J. Boland, J. J. Wang, J. F. Donegan, J. C. Grunlan, G. Moriarty, A. Shmeliov, R. J.

Nicholls, J. M. Perkins, E. M. Grieveson, K. Theuwissen, D. W. McComb, P. D. Nellist and V. Nicolosi, *Science*, 2011, **331**, 568-571.

11. H. Li, Y. Tan, P. Liu, C. Guo, M. Luo, J. Han, T. Lin, F. Huang and M. Chen, *Advanced Materials*, 2016, **28**, 8945-8949.
12. J. Zhou, J. Lin, X. Huang, Y. Zhou, Y. Chen, J. Xia, H. Wang, Y. Xie, H. Yu, J. Lei, D. Wu, F. Liu, Q. Fu, Q. Zeng, C.-H. Hsu, C. Yang, L. Lu, T. Yu, Z. Shen, H. Lin, B. I. Yakobson, Q. Liu, K. Suenaga, G. Liu and Z. Liu, *Nature*, 2018, **556**, 355-359.
13. K. T. Law and P. A. Lee, *Proceedings of the National Academy of Sciences*, 2017, **114**, 6996-7000.
14. B. Sipos, A. F. Kusmartseva, A. Akrap, H. Berger, L. Forro and E. Tutis, *Nat Mater*, 2008, **7**, 960-965.
15. R. Hovden, A. W. Tsen, P. Liu, B. H. Savitzky, I. El Baggari, Y. Liu, W. Lu, Y. Sun, P. Kim, A. N. Pasupathy and L. F. Kourkoutis, *Proceedings of the National Academy of Sciences*, 2016, **113**, 11420-11424.
16. P. Darancet, A. J. Millis and C. A. Marianetti, *Physical Review B*, 2014, **90**, 045134.
17. Q. Zhang, L.-Y. Gan, Y. Cheng and U. Schwingenschlögl, *Physical Review B*, 2014, **90**, 081103.
18. Y. Li, H. Xiao, P. Zhou and J. Cao, *Physics Letters A*, 2019, **383**, 2302-2308.
19. Z. Wang, Y. Shen, Y. Ito, Y. Zhang, J. Du, T. Fujita, A. Hirata, Z. Tang and M. Chen, *ACS Nano*, 2018, **12**, 1571-1579.
20. S. Manzeli, D. Ovchinnikov, D. Pasquier, O. V. Yazyev and A. Kis, *Nature Reviews Materials*, 2017, **2**, 17033.
21. K. Ishizuka, *Ultramicroscopy*, 2001, **90**, 71-83.
22. G. Eda, T. Fujita, H. Yamaguchi, D. Voiry, M. Chen and M. Chhowalla, *ACS Nano*, 2012, **6**, 7311-7317.
23. S. Carr, D. Massatt, S. B. Torrisi, P. Cazeaux, M. Luskin and E. Kaxiras, *Physical Review B*, 2018, **98**, 224102.
24. Y. Luo, Twist angle physics in graphene based van der Waals

heterostructures, PhD Dissertation, Massachusetts Institute of Technology, 2018.

Acknowledgements

This work was supported by MOST 973 of China (2015CB856800) and Natural Science Foundation of China (Grant No. 51821001, 11704245). P. L. is supported by the Program for Professor of Special Appointment (Eastern Scholar) at Shanghai Institutions of Higher Learning. M. C. is sponsored by the Whiting School of Engineering, Johns Hopkins University and National Science Foundation (NSF PD 09-1771).

Competing financial interests: The authors declare no competing financial interests.

Figure Captions

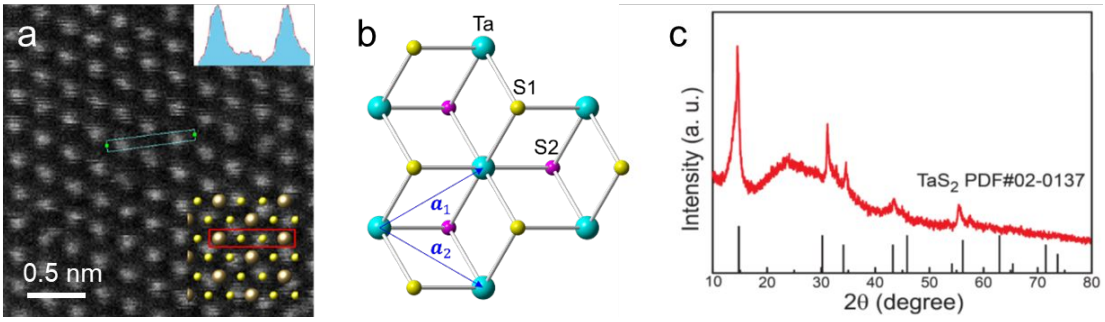

Figure 1 a. HAADF-STEM image from monolayer 1T-TaS_2. Intensity profile extracted from the green frame region exhibits the relative higher scattered signal of Ta atoms on the upper right corner, while does not display the signal of S atoms, indicating the structure of monolayer TaS_2 is 1T phase. The insertion also displays the atomic model of 1T TaS_2. **b.** Illustration of 1T-TaS_2 lattice structure, the first layer S atoms are in yellow, second layer S atoms are in purple, and Ta atoms are in blue. Bravais basis vectors $\overrightarrow{a_1}$, $\overrightarrow{a_2}$ are shown. **c**. X-ray diffraction results of as prepared 1T TaS_2.

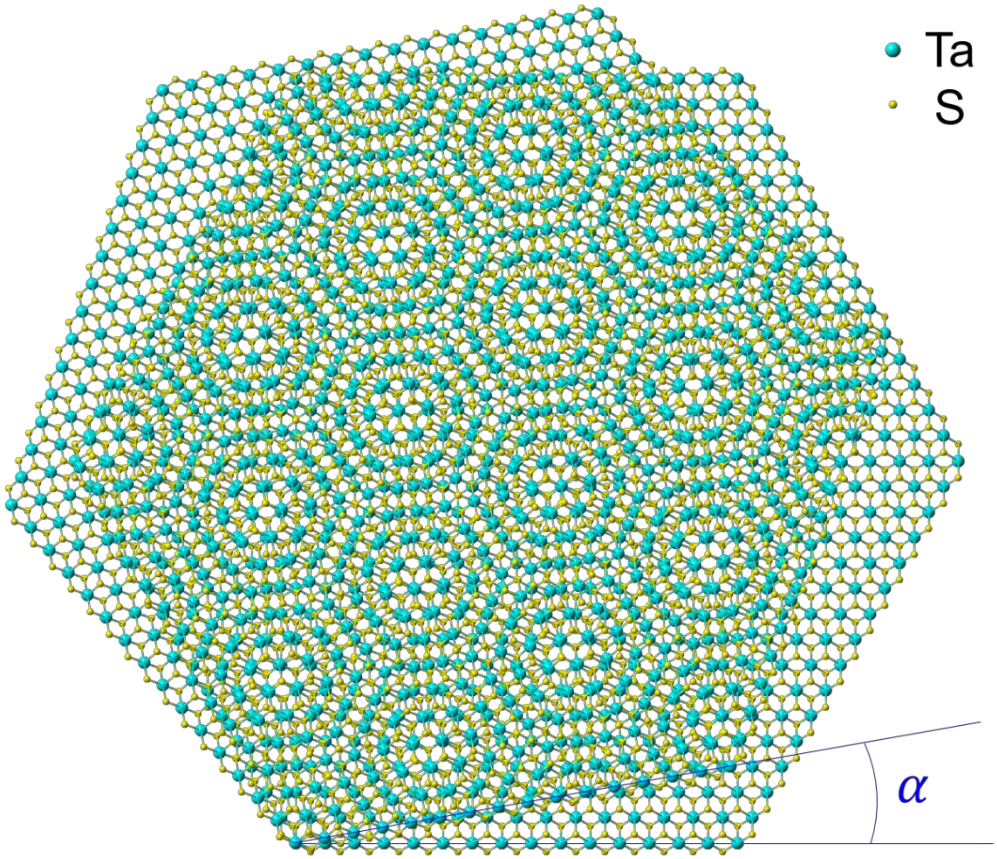

Schematic 1. The twist angle α here is defined as the angle that is twisted in plane from standard AB-stacking 1T-TaS_2

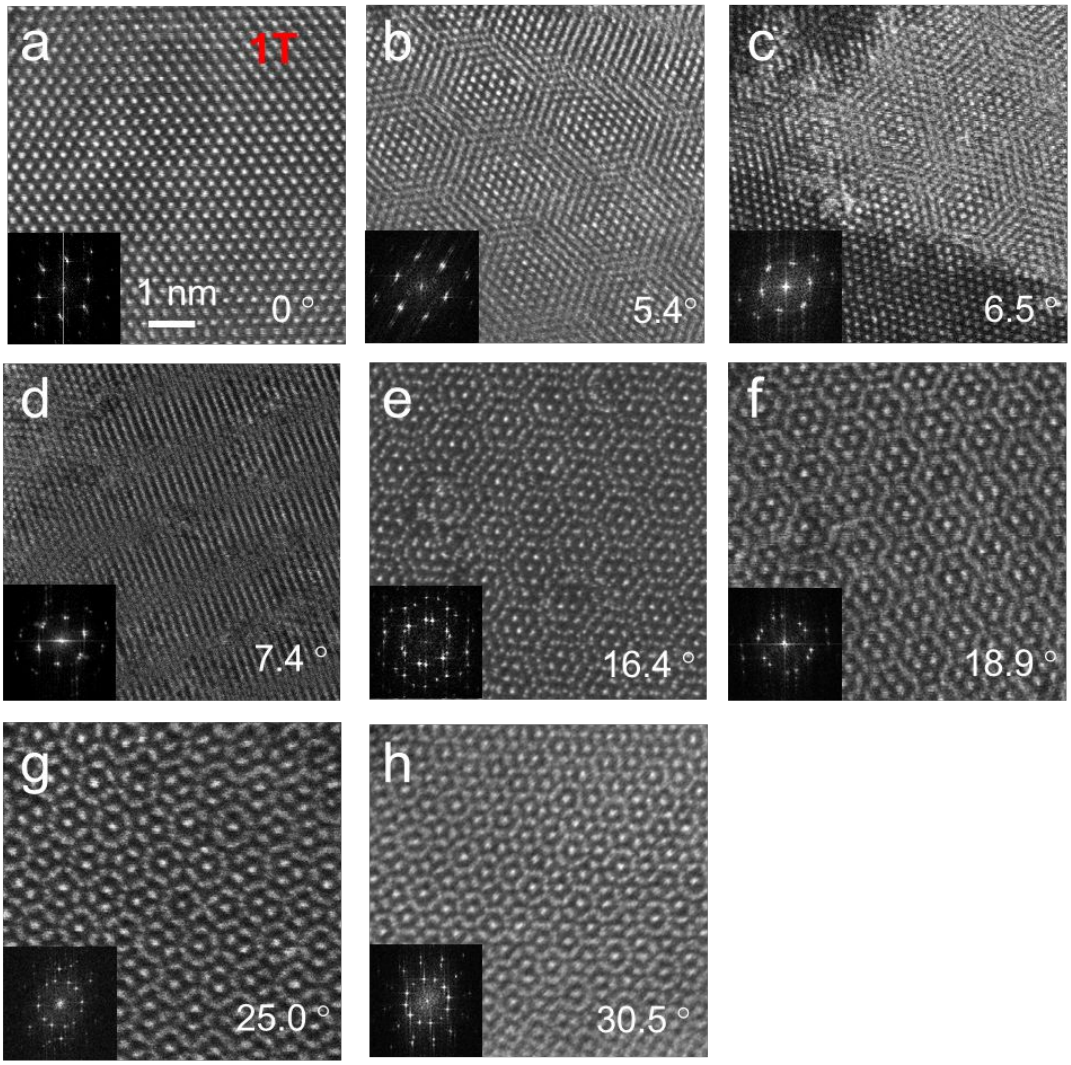

Figure 2. The HAADF-STEM images of 1T-TaS_2 bilayers with different twist angles marked on the right corners. The insets are the Fast Fourier Transform (FFT) patterns derived from the corresponding HAADF-STEM images.

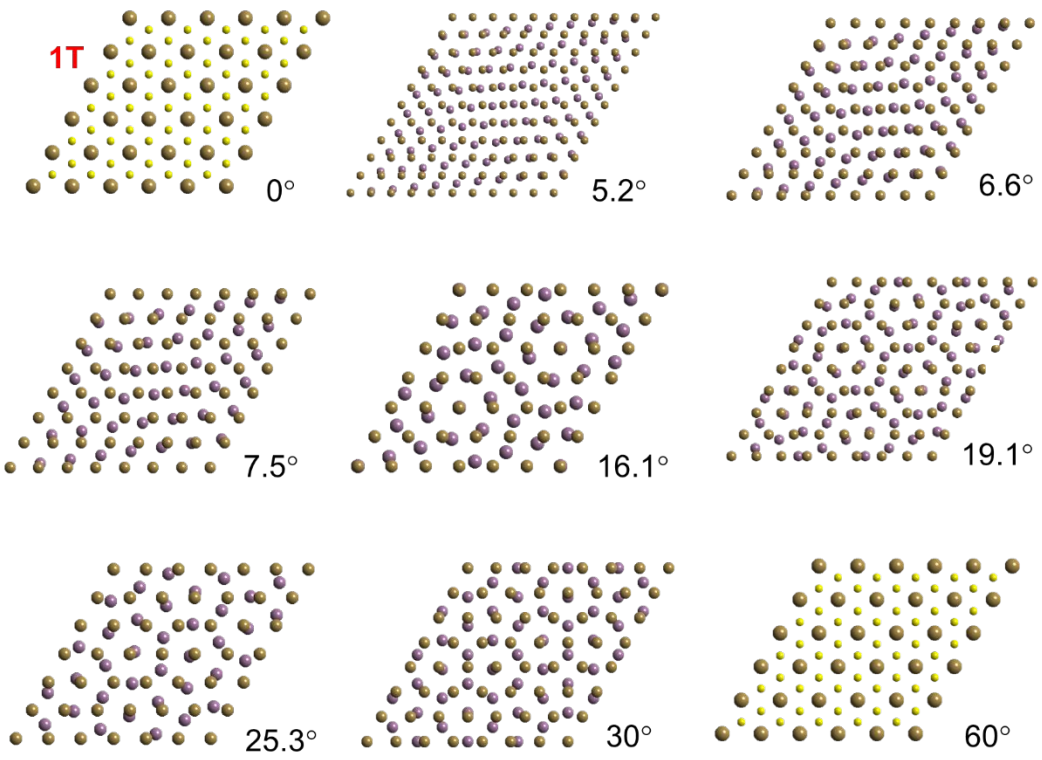

Figure 3. Atomic models of two TaS_2 monolayers with different rotational angle of α in plane used in HREM software. The light-yellow dots represent S atom while the brown and purple dots represent Ta atoms in the first and second layer, respectively. S atoms are not presented other than in 0 and 60^0 twisted models because the atomic structural periodicity can be better revealed by presenting Ta atoms only.

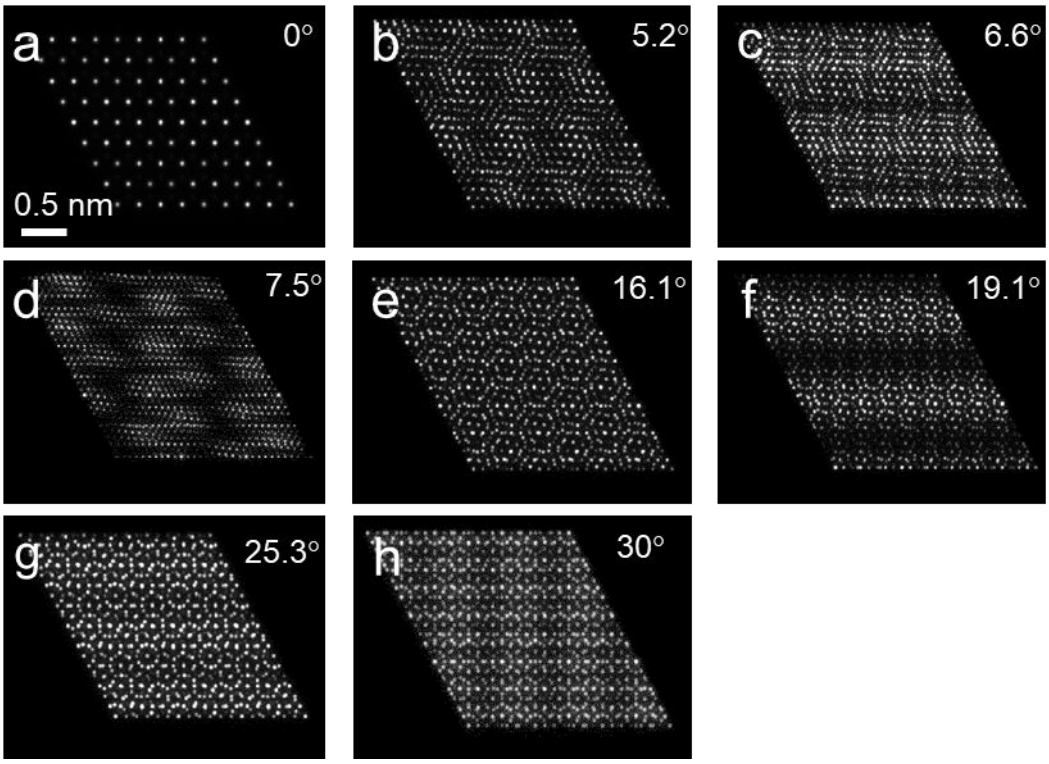

Figure 4. Simulated HAADF-STEM images with different twist angles produced by HREM software based on the Multi-slice Method.

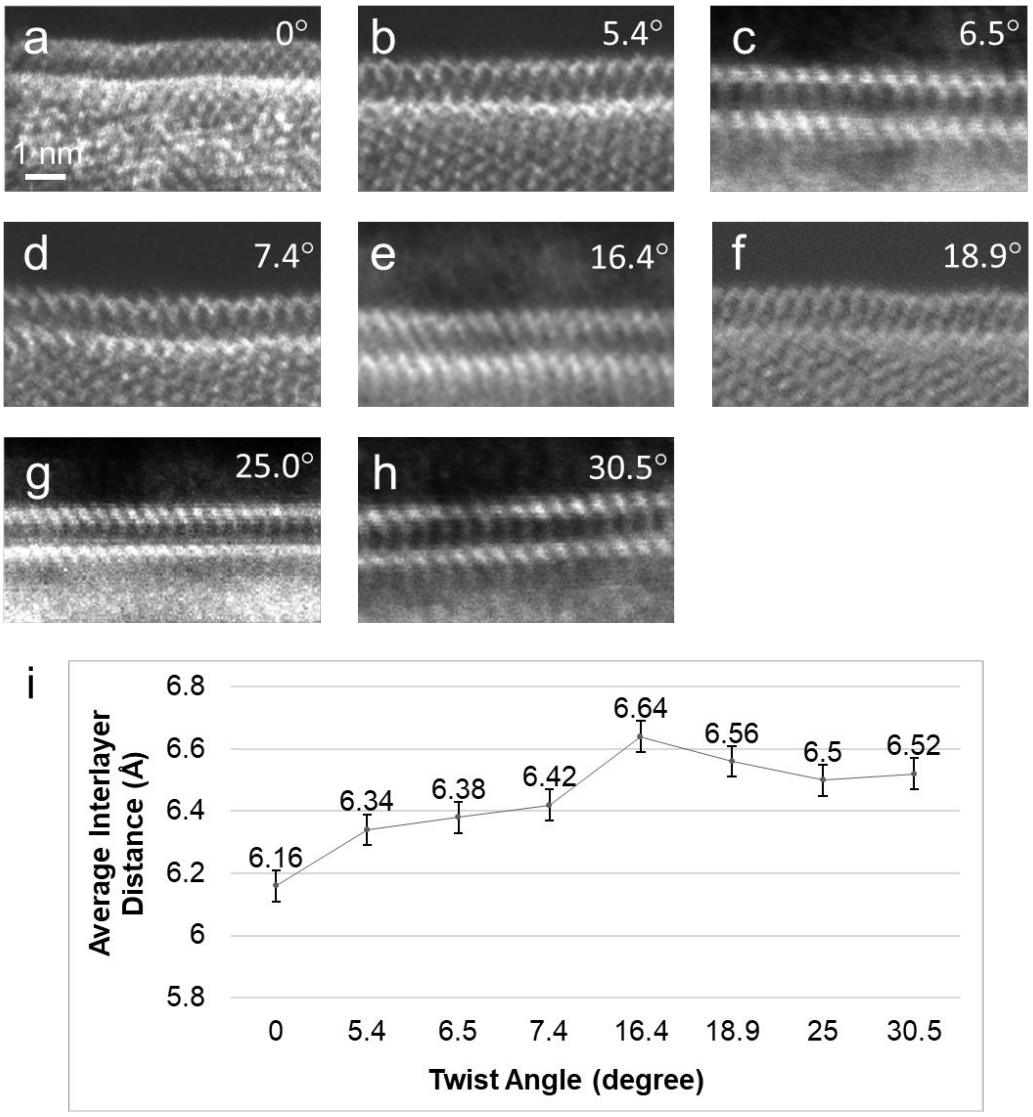

Figure 5. **a-h**. The HAADF-STEM images of folded edges of 1T-TaS_2 bilayers with different twist angles **i.** Average interlayer distance here is the distance between Ta atomic planes measured from a-h through extracting intensity profiles from intensity line scan vertical to the edges.

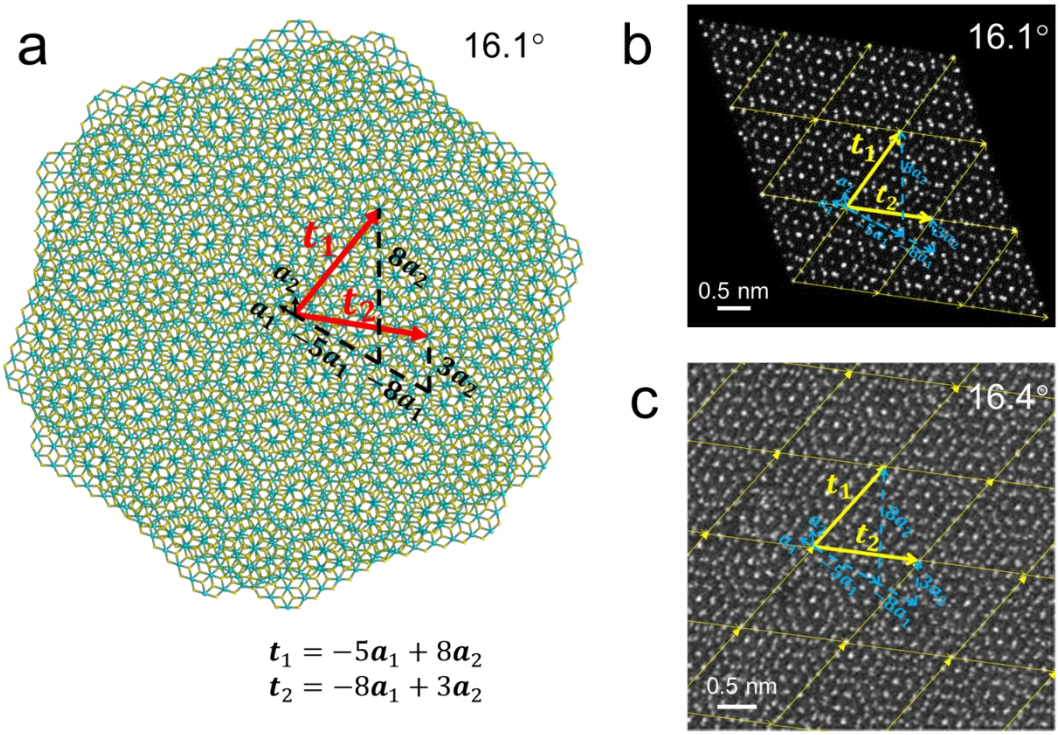

Figure 6. The atomic model, simulated and experimental HAADF-STEM images of 16.1° twisted 1T-TaS_2 bilayer with calculated basis vectors of moiré unit cell $\vec{t}_1$ and $\vec{t}_2$. $\vec{t}_1 = -5\vec{a}_1+8\vec{a}_2$, $\vec{t}_2 = -8\vec{a}_1+3\vec{a}_2$. $\vec{a}_1$ and $\vec{a}_2$ are basic vectors of a untwisted bilayer unit cell. The difference in measured twist angles 16.4° may be from measuring error.

Table 1. Calculated Twist angles ∂ according to equation $\cos(\partial) = \frac{3q^2 - p^2}{3q^2 + p^2}$ $p,q \in Z$, with q equal to integers from 1 to 20, and p equal to integers from 1 to 10. Grey highlighted twist angles are consistent with the experimental observed twisted angles within 0.2° error.

q \ *p*	1	2	3	4	5	6	7	8	9	10
1	60.0									
2	32.2	60.0								
3	21.8	42.1	60.0							
4	**16.4**	32.2	46.8	60.0						
5	13.2	26.0	38.2	49.6	60.0					
6	11.0	21.8	32.2	42.1	51.4	60.0				
7	9.4	**18.7**	27.8	36.5	44.8	52.7	60.0			
8	8.3	16.4	24.4	32.2	39.7	46.8	53.6	60.0		
9	**7.3**	14.6	21.8	28.8	35.6	42.1	48.4	54.3	60.0	
10	**6.6**	13.2	19.7	26.0	32.2	38.2	44.0	49.6	54.9	60.0
11	6.0	12.0	17.9	23.7	29.4	35.0	40.3	45.6	50.6	55.4
12	**5.5**	11.0	16.4	21.8	27.1	32.2	37.2	42.1	46.8	51.4
13	5.1	10.2	15.2	20.1	**25.0**	29.8	34.5	39.1	43.6	47.9
14	4.7	9.4	14.1	18.7	23.3	27.8	32.2	36.5	40.7	44.8
15	4.4	8.8	13.2	17.5	21.8	26.0	30.2	34.2	38.2	42.1
16	4.1	8.3	12.4	16.4	20.5	24.4	28.4	32.2	36.0	39.7
17	3.9	7.8	11.6	15.5	19.3	23.0	26.7	**30.4**	34.0	37.5
18	3.7	7.3	11.0	14.6	18.2	21.8	25.3	28.8	32.2	35.6
19	3.5	7.0	10.4	13.9	17.3	20.7	24.0	27.3	30.6	33.8
20	3.3	6.6	9.9	13.2	16.4	19.7	22.8	26.0	29.1	32.2

Table 2. Calculated basic vectors of moiré unit cells from experimentally observed twist angles, according to equation (5),(6),(7),(8).

Observed twist angle (p,q)	**Basis vectors of moiré unit cell**	**Frequency out of 50 samples**
16.4° (1,4)	$\vec{t}_1 = -5\vec{a}_1+8\vec{a}_2;\ \vec{t}_2 = -8\vec{a}_1+3\vec{a}_2$	5
18.9° (2,7)	$\vec{t}_1 = -9\vec{a}_1+14\vec{a}_2;\ \vec{t}_2 = -14\vec{a}_1+5\vec{a}_2$	3
7.4° (1,9)	$\vec{t}_1 = -5\vec{a}_1+9\vec{a}_2;\ \vec{t}_2 = -9\vec{a}_1+4\vec{a}_2$	2
6.5° (1,10)	$\vec{t}_1 = -11\vec{a}_1+20\vec{a}_2;\ \vec{t}_2 = -20\vec{a}_1+9\vec{a}_2$	3
5.4° (1,12)	$\vec{t}_1 = -13\vec{a}_1+24\vec{a}_2;\ \vec{t}_2 = -24\vec{a}_1+11\vec{a}_2$	3
25.0° (5,13)	$\vec{t}_1 = -9\vec{a}_1+13\vec{a}_2;\ \vec{t}_2 = -13\vec{a}_1+4\vec{a}_2$	1
30.5° (8,17)	$\vec{t}_1 = -25\vec{a}_1+34\vec{a}_2;\ \vec{t}_2 = -34\vec{a}_1+9\vec{a}_2$	1

TOC

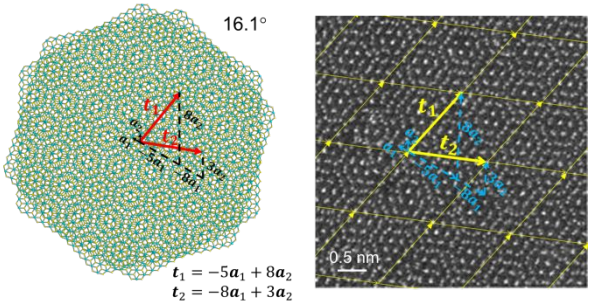

Novelty of the work:

Atomic-scale observations reveal the existence of eight twist commensurate configurations in twisted 1T TaS_2 bilayers synthesized by lithiation exfoliation.